

Investigation on AA5083/AA7075+Al₂O₃ Joint Fabricated by Friction Stir Welding: Characterizing Microstructure, Corrosion and Toughness Behavior

Mehdi Saeidi^a, Mohsen Barmouz^{b*}, Mohammad Kazem Besharati Givi^c

^aYoung Researchers and Elites Club, Science and Research Branch, Islamic Azad University, Tehran, Iran

^bYoung Researchers and Elite Club, Zanzan Branch, Islamic Azad University, Zanzan, Iran

^cDepartment of Mechanical Engineering, University of Tehran, Tehran, Iran

Received: November 18, 2014; Revised: November 24, 2015

The effects of Al₂O₃ reinforcements on microstructure, corrosion and toughness properties of dissimilar aluminum alloys joint fabricated by friction stir welding (FSW) technique were explored in this research. AA5083-H116 and AA7075-T6 were selected as the primary base materials. FSW was conducted with and without reinforcing particles through the joint line. Optical microscopy (OM) confirmed uniform distribution of reinforcement particles within the stir zone (SZ) of Al₂O₃-included specimen. It is demonstrated that the grain size of Al₂O₃-included specimen in SZ was smaller than that of fabricated without Al₂O₃. Besides, a comparative corrosion test was performed to assess the effectiveness of Al₂O₃ particles on corrosion resistance of the joint. The resultant polarization curves gave evidence to a perceptible enhancement in corrosion resistance of the Al₂O₃-included specimen. Fracture toughness, on the other hand, was examined through impact testing. Surprisingly, Al₂O₃-included specimen showed inferior impact toughness due to unsatisfactory bonding between matrix and reinforcements.

Keywords: friction stir welding, aluminum alloy, al₂o₃, corrosion resistance, composite

1. Introduction

Friction stir welding (FSW) is considered as an emerging semi-solid state method for joining a variety of alloys and fabrication of metal matrix composites (MMCs). It was invented at The Welding Institute (TWI) of UK in 1991 and was initially applied to aluminum alloys¹. Automotive and aviation are among the industries that have paid enormous attention to this process². In automotive industry, Al₂O₃/Al MMCs have been used to replace cast iron components such as pistons, engine blocks, cylinder heads, brake calipers and rotors³. Interestingly, over the recent years, a growing attention is paid to the FSW of aluminum matrix composites. Apart from AA6061/Al₂O₃/20p^[4], AA7005/Al₂O₃/10p^[5], AA2124/SiC/25p^[6] and AA2009/SiC/15p^[7] are fit into this category. Pirondi and Collini conducted research into the fracture toughness of AA6061/Al₂O₃ composite. They realized that the embrittlement effect associated with particle reinforcement might be the rational reason behind inferior fracture toughness of composite joint to base material⁸.

Meanwhile, the corrosion behaviors of friction stir welded (FSWed) aluminum alloys have been studied by a number of investigators⁹⁻¹¹. Shen et al.¹¹ determined corrosion resistance of 5083/6082 joint in NaCl solution. They discovered that the corrosion resistance of FSWed joints was higher than those of both parent materials. On the other hand, Devaraju & Kumar¹² reported improved corrosion resistance of AA6061/SiC composite layer produced by friction stir processing (FSP) and they claimed that it could be attributed

to the well-bonding between the reinforcements and matrix and homogeneously distribution of fillers.

More recently, based on a novel approach, Bahrami et al.¹³ applied FSW for joining of two AA7075 plates using SiC reinforcements along the joint line and found promising results from the standpoint of impact toughness. They reported that excellent bonding between reinforcements and the substrate was the reason of positive effect of SiC particles on impact energy absorption. No study to date, however, addressed the joining of dissimilar aluminum alloys based on the foregoing method. Accordingly, the main purpose of this study is to examine the effects of Al₂O₃ particles on the microstructure, corrosion properties, and fracture toughness of AA7075/AA5083 joint performed via FSW. Excellent corrosion resistance of AA7075-T6 and AA5083-H116 aluminum alloys, along with a unique combination of mechanical properties are the reasons why authors have picked up these alloys as the substrates¹⁴⁻¹⁶. Moreover, in some industries such as marine and aviation, sometimes a mixture of various properties is required, particularly with respect to the existed environments. Accordingly, joining high strength and high corrosion resistance alloys could be crucial. Obviously in such industries, metallurgical and mechanical properties of the welded joints are very critical.

2. Experimental Procedure

In this study, 5 mm thick AA5083-H116 and AA7075-T6 aluminum alloy sheets with the chemical composition shown in Table 1 were employed. Prior to use, base materials were

*e-mail: mbarmouz@ut.ac.ir, m.saeidi@srbiau.ac.ir

Table 1. Chemical composition of the base materials.

Base materials	Mg	Zn	Mn	Fe	Cu	Si	Ti	Al
AA5083-H116	4.45	0.04	0.44	0.33	0.07	0.22	0.05	Balance
AA7075-T6	2.4	5.7	0.17	0.18	1.55	0.06	0.01	Balance

cut into 200 × 50 × 5 mm strips. After cutting, profiles were machined on the adjoining side of each strip in dimensions of 2 mm in depth and 0.5 mm in width in a way that when they were put together the groove formed between two strips. Then with the aim of reinforcing the stir zone (SZ), Al₂O₃ nanoparticles were put along the joint line inside the groove. The properties and micrograph of the as-received Al₂O₃ reinforcing particles are provided in Table 2 and Figure 1, respectively. The FSW tool was fabricated from H13 hot work steel. Apart from dimensions (in mm), side and top views of the tool are demonstrated in Figure 2. While AA5083-H116 alloy was fixed on advancing side, FSW was conducted at rotational and traveling speeds of 800 rpm and 50 mm/min, respectively.

Potentiodynamic polarization measurements were performed according to the ASTM G69, in a typical three-electrode cell containing a stainless steel plate as an auxiliary electrode¹⁷. The potentiodynamic experiments were carried out from -1 V to +1 V with respect to the open circuit potential (OCP) at a scan rate of 1 mV/s. The OCP was monitored for 30 min in 3.5 wt% NaCl solution. Toward this end, one EG&G Princeton applied research Potentiostat/Galvanostat model 273A was employed. A Saturated Calomel Electrode (SCE) was utilized as a reference electrode. In order to boost the experimental results correctness, three corrosion tests were conducted at room temperature (25 °C) on each sample and the electrolyte was changed after each experiment. On the other hand, impact tests were performed at room temperature employing CEAST Resil Impactor machine. Following instructions in ASTM E23, Izod-type Impact test specimens were prepared and tested¹⁸. The average value of three specimens was reported as the result of each impact test.

The specimens for metallographic and corrosion examinations were cross-sectioned perpendicular to the welding direction and prepared for microstructural investigation. The specimens before preparation are shown in Figure 3. The corrosion specimens were polished but not as much as metallographic samples. Following preparation, metallographic specimens were etched 15 s with Poulton and Keller reagents. Recent reagents are commonly used as etchant for AA5083 and AA7075, respectively¹⁹. Moreover, scanning electron microscopy (SEM) and optical microscopy (OM) techniques were employed for microstructural characterization. It is worth to know that the linear intercept method was used to measure the specimens' grain size.

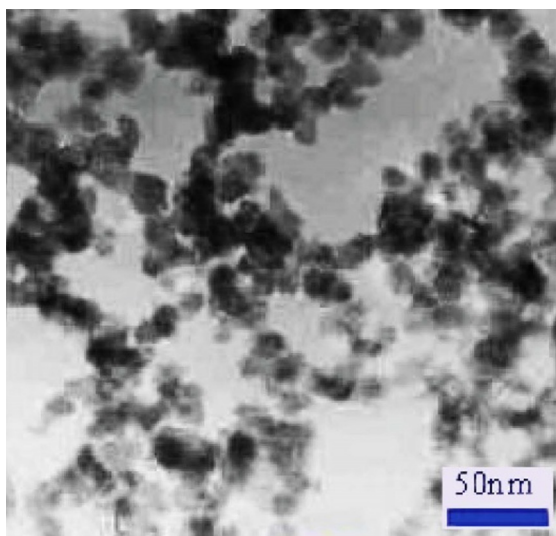
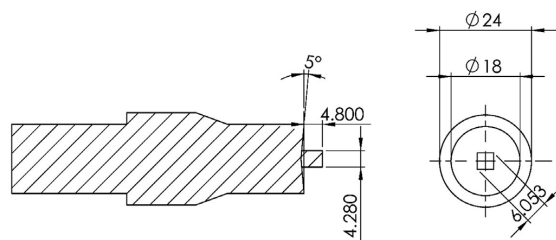
3. Results and Discussion

3.1. Macro and microstructural observations

It is reported by Johnson & Threadgill²⁰ that the locations of two dissimilar alloys exert a significant effect on material flow pattern and the resultant weld quality. They noticed that better welds produced when low-strength material placed on the advancing side. This is why AA5083-H116 was situated on advancing side in this research. Macrostructural sections

Table 2. Properties of Al₂O₃ nano-particles.

Purity	Particle size (APS)	Type	Color
99+%	20 nm	Gamma	White

**Figure 1.** Micrograph of the as-received Al₂O₃ nanoparticles.**Figure 2.** Side and top views of FSW tool.

are exhibited in Figure 4 which materials flows are evident in these macrographs. The absence of tangible defects in stir zones suggests suitable material flow around the pin tool and this implies the soundness of FSWed joints. Formation of elliptical nugget zone was seen in the middle of the joint for all the samples. The shape of SZ depends on the processing parameters, tool geometry, work-piece temperature and thermal conductivity of the material²¹. Since the both nugget zones are extremely similar in appearance, it could be inferred that the addition of reinforcement particles does not have a major effect on the nugget's shape.

Various areas of the Al₂O₃-free joint are addressed in Figure 5, namely: SZ, heat affected zone (HAZ), and base material. It is worth to mention that thermomechanically affected zone (TMAZ), however, is barely discernible in Figure 5. Regarding the SZ of unreinforced joint and base material structures, it was observed that grain size is decreased

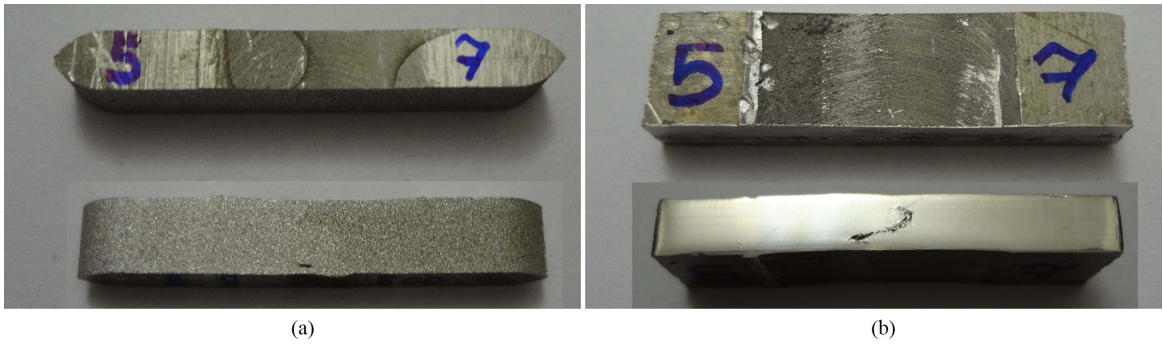


Figure 3. specimens' shape used for (a) metallography and (b) corrosion.

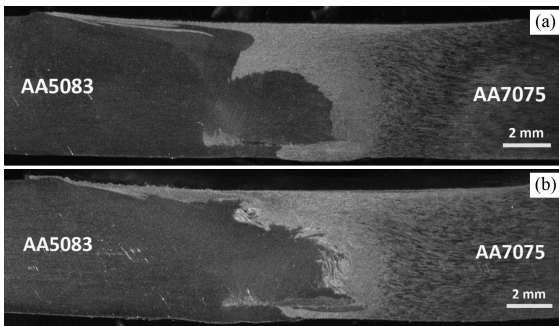


Figure 4. Macrographs of FSWed specimens: (a) Al_2O_3 -free; (b) Al_2O_3 -included.

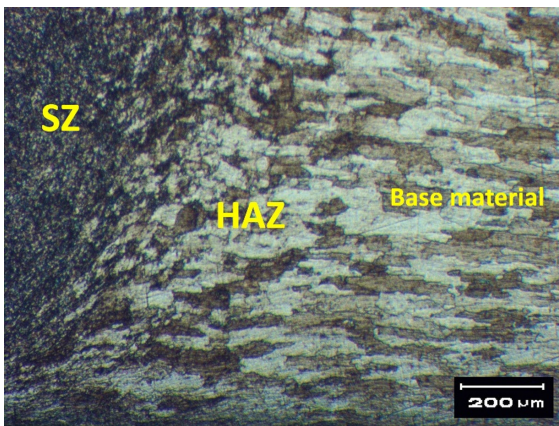


Figure 5. Formation of different areas in Al_2O_3 -free joint.

considerably from 22 and 160 μm in AA5083 and AA7075, respectively; to 6 μm .

Higher magnification of SZ microstructure for this sample including fine equiaxed grains is presented in Figure 6a. As a matter of fact, during friction stir welding, material undergoes severe plastic deformation at elevated temperature which results in the formation of new nucleation sites which make the grains size smaller. This phenomenon is known as dynamic recrystallization (DRX) which occurs during straining of metals at high temperature, characterized by a nucleation rate of low dislocation density grains and a posterior growth rate that can produce a homogeneous grain size when equilibrium is reached²²⁻²⁴. Figure 6b, on the

other hand, shows the SZ microstructure of Al_2O_3 -included specimen which implies that grain size of this specimen is smaller than that of Al_2O_3 -free specimen. The main reason behind this phenomenon is the existence of reinforcement particles acting as nucleation sites. Moreover, they suppress grain boundaries movements and therefore limit grain coarsening which this phenomenon is known as pinning effect²¹. As a result of pinning effect along with dynamic recrystallization, more and smaller grains are formed within the SZ of Al_2O_3 -included specimen. It is noticeable that the input heat through the FSW is the effective factor to anneal the grains and make increase in grain size but the abovementioned factors are dominative in governing the grain size variation for this specimen.

Figure 7 shows the SEM image of the stir zone for the Al_2O_3 included specimen which is dealing with uniform distribution of Al_2O_3 particles in the processed area. According to Figure 7, Al_2O_3 cluster size varied in the range of 160 to 290 nm. Based on Zener equation, $d_z = 4r/3v_p$, limiting grain size (d_z) was calculated in the Al_2O_3 -included specimen²¹. In this equation, r and v are the radius and volume fraction of reinforcements, respectively. The volume fraction of the reinforcement was calculated based on the proportion of groove area to pin area which measured to be 0.03. The measured limiting grain sizes were 5.3 and 9.6 μm with the average of 7.3 μm . Comparing to the grain size measured based on linear intercept method in metallography section, there is no big difference.

3.2. Corrosion behavior

Figure 8 illustrates the polarization diagram for FSWed specimens. Along with corrosion potentials (E_{corr}) and exchange current densities (I_{corr}) of FSWed specimens, E_{pit} was also extracted from the diagram. To draw a comparison, E_{corr} and I_{corr} of the base materials are provided in Table 3. For the FSWed specimen, small grains formed within the SZ resulted in grain boundaries fraction increment which is thermodynamically susceptible to corrosion. Therefore, finer microstructure of the FSWed zone causes poorer corrosion behavior compared to the base metal²⁵. From Table 3, it is clear that the corrosion resistances of the both FSWed specimens are less than that of each base material.

Grain sizes in the SZ of reinforced and unreinforced specimens were 4 and 6 μm , respectively. However, I_{corr} obtained from reinforced specimen was negligibly lower

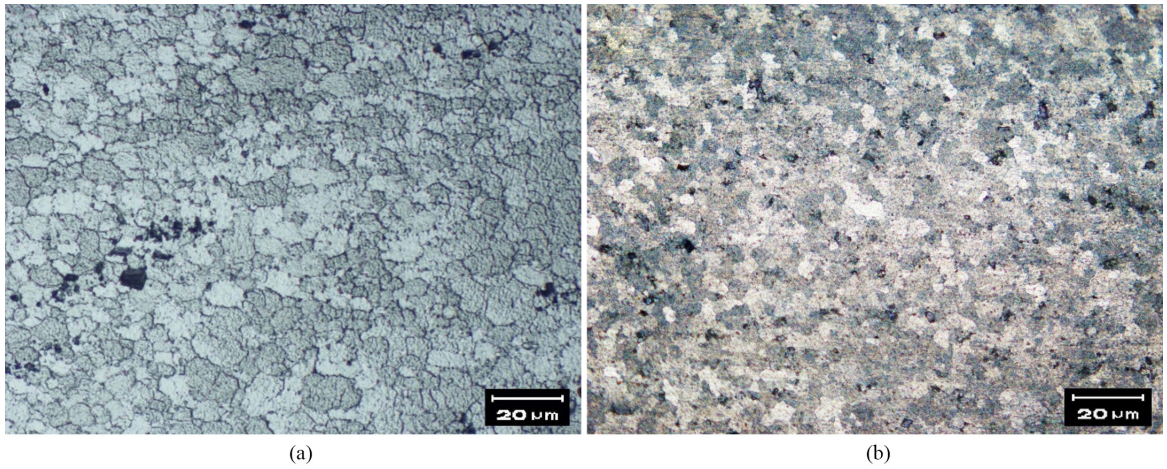


Figure 6. SZ micrograph of the (a) Al₂O₃-free and (b) Al₂O₃-included specimens.

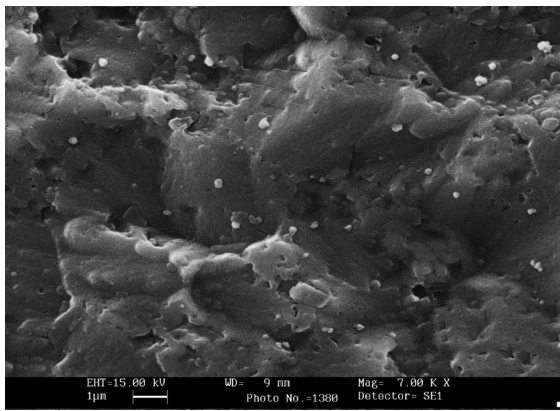


Figure 7. SEM image of the Stir zone for the Al₂O₃-included specimen.

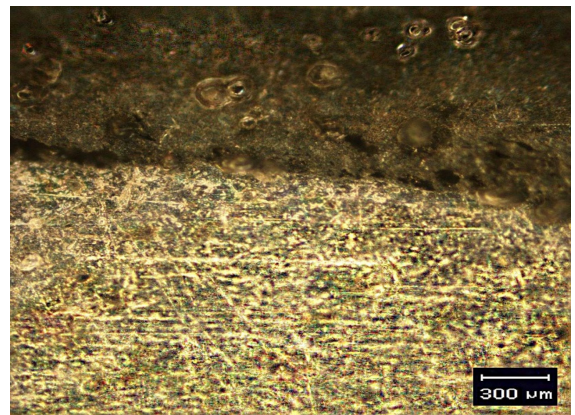


Figure 9. OM micrograph of Al₂O₃-free corroded surface.

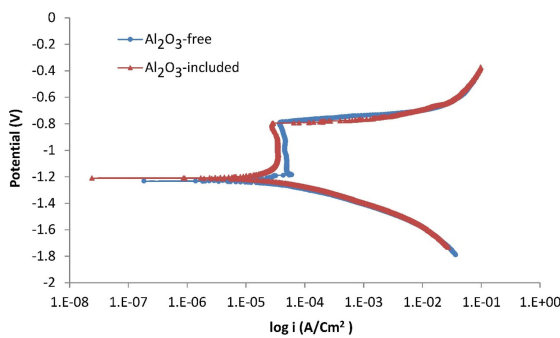


Figure 8. Polarization curves obtained from the SZ of Al₂O₃-free and Al₂O₃-included specimens.

Table 3. Corrosion potentials and exchange current densities of FSWed joints and primary alloys.

Sample	E _{corr} (V)	I _{corr} (A/cm ²)	E _{pit} (V)
Al ₂ O ₃ -free weld	-1.27	5 × 10 ⁻⁵	-0.815
Al ₂ O ₃ -included weld	-1.24	3 × 10 ⁻⁵	-0.817
AA5083-H116	-1.16	1 × 10 ⁻⁵	-
AA7075-T6	-1.13	2 × 10 ⁻⁵	-

than that of the unreinforced specimen. In other words, the corrosion resistance of Al₂O₃-included specimen was slightly superior to that of the Al₂O₃-free specimen. This result is in good agreement with that of gained by Devaraju & Kumar¹² in the case of 6061-T6/SiCp composite produced via FSP. At mentioned work the improved corrosion resistance of SZ was attributed to uniform distribution of reinforcement particles as well as satisfactory bonding between reinforcements and the matrix. In addition, both specimens showed almost identical E_{pit}. Table 3. It is understood that the Al₂O₃ reinforcements usually do not have a significant effects on pitting potentials in chloride solutions³.

Figure 9 shows the optical micrograph of corroded surface in Al₂O₃-free specimen. Brighter appearance associated with AA5083 confirms its superior corrosion resistance to AA7075. The 7xxx wrought alloys, because of their zinc contents, are anodic to aluminum alloys of other series. Besides, the presence of copper element in AA7075 is another reason which is responsible for its weak corrosion resistance³. Taking a closer look to Figure 9 revealed that chemically attacked regions are mainly located around precipitates. Indeed, corrosion potential of the second phase is not the same as the parent phase³. Accordingly, precipitates in heat-treatable side of the joint i.e, AA7075-T6, are preferable sites for

corrosion attack. Paglia & Buchheit²⁶ observed similar result and ascribed it to wide precipitate-free zones and coarse precipitates such as Mg [Zn₂, AlCu] and MgAlCu in 7075 aluminum alloy. However, as a non-heat-treatable

aluminum alloy, no precipitate is formed in AA5083 section. Consequently, as a result of homogenous microstructure, corrosion attacks are avoided in AA5083 side of the joint.

3.3. Fracture toughness

Impact test results are presented in Figure 10. It was expected that Al₂O₃-included joint must had higher fracture toughness than Al₂O₃-free specimen due to this fact that former one had smaller grain size and consequently higher strength. However, on the contrary; at current work the specimen FSWed with presence of the Al₂O₃ particles showed the least fracture toughness. This is because of the fact that although adding the Al₂O₃ particles inside the metallic matrix improves the strength and reduces the grain size but presence of the nano-filler inside the matrix increases the possibility of crack propagation as a result of impact test.

Figure 11 shows macroscopic fracture surfaces of impact specimens. As it is indicated, dark surfaces depict the presence of Al₂O₃ particles in Figure 11b. At a higher magnification, fractured surfaces were further studied via SEM in Figure 12. Fracture micrograph of Al₂O₃-free specimen is indicative of its brittle fracture as well.

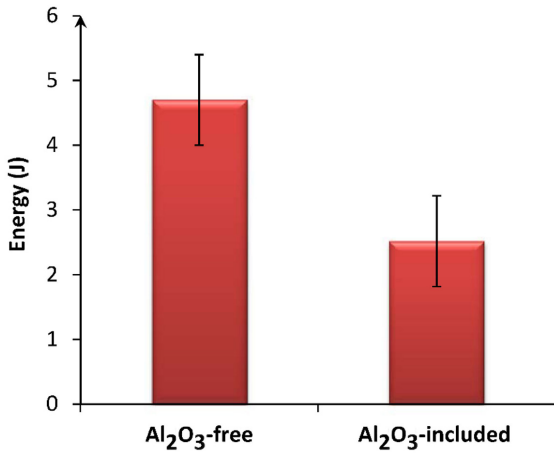


Figure 10. Impact energy of Al₂O₃-free and Al₂O₃-included specimens.

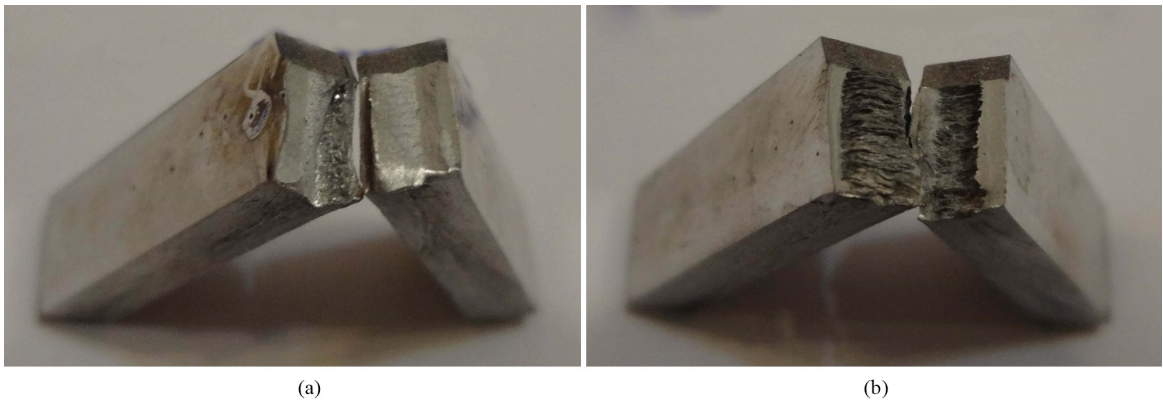


Figure 11. Fracture surface of impact test specimens: (a) Al₂O₃-free; (b) Al₂O₃-included.

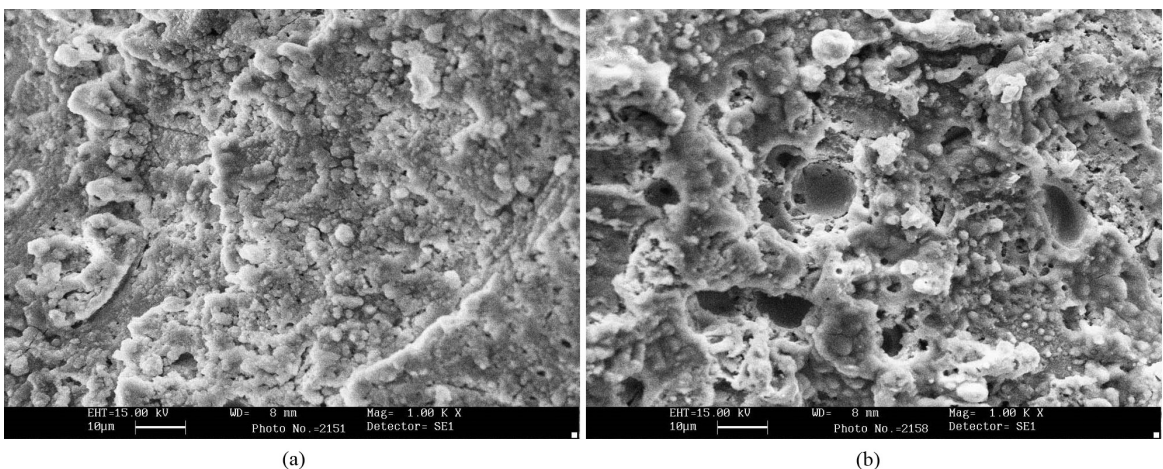


Figure 12. SEM image of fracture surface for impact test of the specimens: (a) Al₂O₃-free; (b) Al₂O₃-included.

Indeed, the absence of voids and dimples on fracture surface suggests brittle mode. On the other hand, reinforcement particles are obviously emerged in fracture micrograph of Al₂O₃-included specimen (Figure 12b). As a matter of fact, loose bonding of reinforcements with the substrate and probable clusters aggregation reduced the required fracture energy. This result is against Bahrami et al.¹³ achievements in the case of AA7075 joint reinforced with SiC nanoparticles. As it is addressed, the reason why they found higher fracture toughness for SiC-included specimen was the excellent bonding between reinforcements and the matrix. Thus, the inferiority of current bonding with respect to the foregoing one could be because of higher wettability of SiC particles with matrix compared to that of Al₂O₃. Therefore, in this case the de-bondings between the matrix and Al₂O₃ powders act as crack propagation sites which weaken the impact strength of the specimen.

4. Conclusions

In current study, Al₂O₃ nanoparticles were compressed embedded into the joint path of AA5083 and AA7075 sheets. For comparison, friction stir welding was conducted without incorporating particles and in brief following results could be mentioned:

1. Joining the AA5083 and AA7075 using FSW leads to dramatic reduction of grain size in the stir zone and this reduction in grain size was more tangible for the specimens containing Al₂O₃ as reinforcement particles.
2. Sound and defect free weld was performed in spite of presence of reinforcements in the stir zone.
3. Presence of Al₂O₃ particles leads to improve the corrosion resistance of the joint when compared to that of welded joint without reinforcements.
4. Fracture toughness of the reinforced FSW was diminished compared to unreinforced joint which could be due to the weak interface of reinforcements and substrate and probable clusters aggregation.

Acknowledgements

The authors gratefully acknowledge the assistance of the Azad University (IAU) and University of Tehran laboratories. It is quite a justice to give a galaxy of heartfelt thanks to all memorable attempts of Dr. Mohammad Kazem Besharati Givi.

References

1. Mishra RS and Ma ZY. Friction stir welding and processing. *Materials Science and Engineering R Reports*. 2005; 50(1–2):1–78. <http://dx.doi.org/10.1016/j.msere.2005.07.001>.
2. Yau Y, Hussain A, Lalwani R, Chan H and Hakimi N. Temperature distribution study during the friction stir welding process of Al2024-T3 aluminum alloy. *International Journal of Minerals, Metallurgy, and Materials*. 2013; 20(8):779-787. <http://dx.doi.org/10.1007/s12613-013-0796-2>.
3. Cramer SD and Covino BS. *Corrosion: fundamentals, testing, and protection*. Materials Park: ASM International; 2003. ASM Handbook, 13A.
4. Ceschini L, Boromei I, Minak G, Morri A and Tarterini F. Microstructure, tensile and fatigue properties of AA6061/20vol.%Al2O3p friction stir welded joints. *Composites. Part A, Applied Science and Manufacturing*. 2007; 38(4):1200-1210. <http://dx.doi.org/10.1016/j.compositesa.2006.06.009>.
5. Ceschini L, Boromei I, Minak G, Morri A and Tarterini F. Effect of friction stir welding on microstructure, tensile and fatigue properties of the AA7005/10vol.%Al2O3p composite. *Composites Science and Technology*. 2007; 67(3-4):605-615. <http://dx.doi.org/10.1016/j.compscitech.2006.07.029>.
6. Uzun H. Friction stir welding of SiC particulate reinforced AA2124 aluminium alloy matrix composite. *Materials & Design*. 2007; 28(5):1440-1446. <http://dx.doi.org/10.1016/j.matdes.2006.03.023>.
7. Feng AH, Xiao BL and Ma ZY. Effect of microstructural evolution on mechanical properties of friction stir welded AA2009/SiCp composite. *Composites Science and Technology*. 2008; 68(9):2141-2148. <http://dx.doi.org/10.1016/j.compscitech.2008.03.010>.
8. Pirondi A and Collini L. Analysis of crack propagation resistance of Al–Al2O3 particulate-reinforced composite friction stir welded butt joints. *International Journal of Fatigue*. 2009; 31(1):111-121. <http://dx.doi.org/10.1016/j.ijfatigue.2008.05.003>.
9. Kang J, Fu R, Luan G, Dong C and He M. In-situ investigation on the pitting corrosion behavior of friction stir welded joint of AA2024-T3 aluminium alloy. *Corrosion Science*. 2010; 52(2):620-626. <http://dx.doi.org/10.1016/j.corsci.2009.10.027>.
10. Venugopal T, Srinivasa Rao K and Prasad Rao K. Studies on friction stir welded AA 7075 aluminum alloy. *Transactions of the Indian Institute of Metals*. 2004; 57(6):659-663.
11. Shen C, Zhang J and Ge J. Microstructures and electrochemical behaviors of the friction stir welding dissimilar weld. *Journal of Environmental Sciences*. 2011; 23(Suppl):32-35. [http://dx.doi.org/10.1016/S1001-0742\(11\)61072-3](http://dx.doi.org/10.1016/S1001-0742(11)61072-3). PMID:25084589.
12. Devaraju A and Kumar A. Dry sliding wear and static immersion corrosion resistance of aluminum alloy 6061-T6/SiC p metal matrix composite prepared via friction stir processing. *International Journal of Applied Research In Mechanical Engineering*. 2011; 1(2):62-68.
13. Bahrami M, Helmi N, Dehghani K and Givi MKB. Exploring the effects of SiC reinforcement incorporation on mechanical properties of friction stir welded 7075 aluminum alloy: fatigue life, impact energy, tensile strength. *Materials Science and Engineering A*. 2014; 595:173-178. <http://dx.doi.org/10.1016/j.msea.2013.11.068>.
14. Hatamleh O, Lyons J and Forman R. Laser and shot peening effects on fatigue crack growth in friction stir welded 7075-T7351 aluminum alloy joints. *International Journal of Fatigue*. 2007; 29(3):421-434. <http://dx.doi.org/10.1016/j.ijfatigue.2006.05.007>.
15. Hatamleh O, Singh PM and Garmestani H. Corrosion susceptibility of peened friction stir welded 7075 aluminum alloy joints. *Corrosion Science*. 2009; 51(1):135-143. <http://dx.doi.org/10.1016/j.corsci.2008.09.031>.
16. Choi D-H, Ahn B-W, Quesnel DJ and Jung S-B. Behavior of β phase (Al₃Mg₂) in AA 5083 during friction stir welding. *Intermetallics*. 2013; 35(0):120-127. <http://dx.doi.org/10.1016/j.intermet.2012.12.004>.
17. American Society for Testing and Materials – ASTM. *Annual Book of ASTM Standards*. West Conshohocken: ASTM; 2005. Section 03.02, G69-03.

18. American Society for Testing and Materials – ASTM. *E23-09: standard test method for notched bar impact testing of metallic materials*. West Conshohocken: ASTM; 2009. Annual Book of ASTM Standards.
19. Dolatkhan A, Golbabaee P, Besharati Givi MK and Molaiekiya F. Investigating effects of process parameters on microstructural and mechanical properties of Al5052/SiC metal matrix composite fabricated via friction stir processing. *Materials & Design*. 2012; 37(0):458-464. <http://dx.doi.org/10.1016/j.matdes.2011.09.035>.
20. Johnson R and Threadgill P. Friction stir welding of magnesium alloys. *Materials Science Forum*. 2003; 419-422:365-370. <http://dx.doi.org/10.4028/www.scientific.net/MSF.419-422.365>.
21. Zohoor M, Besharati Givi MK and Salami P. Effect of processing parameters on fabrication of Al–Mg/Cu composites via friction stir processing. *Materials & Design*. 2012; 39:358-365. <http://dx.doi.org/10.1016/j.matdes.2012.02.042>.
22. Morisada Y, Fujii H, Nagaoka T and Fukusumi M. MWCNTs/AZ31 surface composites fabricated by friction stir processing. *Materials Science and Engineering A*. 2006; 419(1-2):344-348. <http://dx.doi.org/10.1016/j.msea.2006.01.016>.
23. El-Rayes MM and El-Danaf EA. The influence of multi-pass friction stir processing on the microstructural and mechanical properties of Aluminum Alloy 6082. *Journal of Materials Processing Technology*. 2012; 212(5):1157-1168. <http://dx.doi.org/10.1016/j.jmatprotec.2011.12.017>.
24. Humphreys F and Hatherly M. *Recrystallization and related annealing phenomena*. Oxford: Elsevier; 2004. 658 p.
25. Fahimpour V, Sadmezhaad SK and Karimzadeh F. Corrosion behavior of aluminum 6061 alloy joined by friction stir welding and gas tungsten arc welding methods. *Materials & Design*. 2012; 39(0):329-333. <http://dx.doi.org/10.1016/j.matdes.2012.02.043>.
26. Paglia CS and Buchheit RG. A look in the corrosion of aluminum alloy friction stir welds. *Scripta Materialia*. 2008; 58(5):383-387. <http://dx.doi.org/10.1016/j.scriptamat.2007.10.043>.